

Global alignment of solution-based single-wall carbon nanotube films via machine-vision controlled filtration

Joshua S. Walker,[†] Jeffrey A. Fagan,[‡] Adam J. Biacchi,[¶] Valerie A. Kuehl,[§]
Thomas A. Searles,^{||} Angela R. Hight Walker,[¶] and William D. Rice^{*,†}

[†]*Department of Physics, University of Wyoming, Laramie, WY, 82071*

[‡]*National Institute of Standards and Technology, Materials Science and Engineering
Division, Gaithersburg, MD, 20899*

[¶]*National Institute of Standards and Technology, Nanoscale Device and Characterization
Division, Gaithersburg, MD, 20899*

[§]*Department of Chemistry, University of Wyoming, Laramie, WY, 82071*

^{||}*Department of Physics & Astronomy, Howard University, Washington, DC, 20059*

E-mail: wrice2@uwyo.edu

Abstract

Over the past decade, substantial progress has been made in the chemical control (chiral enrichment, length sorting, handedness selectivity, and filling substance) of single-wall carbon nanotubes (SWCNTs). Recently, it was shown that large, horizontally-aligned films can be created out of post-processed SWCNT solutions. Here, we use machine-vision automation and parallelization to simultaneously produce globally-aligned SWCNT films using pressure-driven filtration. Feedback control enables filtration to occur with a constant flow rate that not only improves the nematic ordering of the SWCNT films, but also provides the ability to align a wide range of SWCNT types and on a variety of nanoporous membranes using the same filtration parameters. Using polarized optical spectroscopic techniques, we show that under standard implementation, meniscus combing produces a two-dimensional radial SWCNT alignment on one side of the film. After we flatten the meniscus through silanation, spatially-resolved nematicity maps on both sides of the SWCNT film reveal global alignment across the entire structure. From experiments changing ionic strength and membrane charging, we provide evidence that the SWCNT alignment mechanism stems from an interplay of intertube interactions and ordered membrane charging. This work opens up the possibility of creating globally-aligned SWCNT film structures for a new-generation of nanotube electronics and optical control elements.

Keywords

Nematic ordering, 1D crystals, single-wall carbon nanotubes, directional charging

Significant interest in one-dimensional (1D) nanocrystals (NCs) follows from their highly anisotropic properties of electrical and thermal transport, optical absorption, radiative emis-

sion, and conduction. Typically, physical attributes observed in these NCs are significantly enhanced along the extended 1D crystal axis relative to the short axes, the latter often

serving to impose strict quantum mechanical boundary conditions on the band structure. Researchers have utilized the anisotropic nature of 1D NCs in polymer chains, liquid crystals, inorganic crystals, and carbonaceous ribbons (graphene, e.g.), and nanotubes to explore physically-interesting 1D behaviors like Luttinger liquids,¹⁻³ time-reversal-invariant Majorana chains,^{4,5} Wigner crystals,⁶ ultrastrong light-matter coupling,^{7,8} high-harmonic generation,⁹ Aharonov-Bohm physics,^{10,11} intersubband plasmons,¹² and topological insulators.¹³ Additionally, 1D NCs have been envisioned in a wide range of technologically-important applications, such as high current-carrying capacity conductors,^{14,15} rectifiers,¹⁶ far-infrared polarizers¹⁷ and detectors,¹⁸ gas and molecular sensing,^{19,20} flexible electronics,²¹ photoelectron emission,²² and directional heat transport.²³ Consequently, enhancing these anisotropic effects by aligning 1D NCs along a common axis via an easy-to-control mechanical, electrical, or magnetic external force is highly desirable. However, the high degree of van der Waals interactions per unit mass in these nanosystems promotes particle aggregation, which contributes to the difficulty in creating globally-aligned macroscopic films of 1D NCs.

Among the major 1D NC groupings, single-wall carbon nanotubes (SWCNTs) are particularly difficult to reproducibly align, especially after they have gone through solution-based processing. Despite the well-known challenges involved in nanotube preparation, strong interest remains in working with SWCNTs due to their unique band structures and exemplary physical properties.²⁴ Substantial research into chemically processing SWCNTs to achieve and enhance these superlative behaviors has produced significant breakthroughs in chiral and type enrichment,²⁵⁻²⁸ length sorting,²⁹ tube filling with atoms and molecules,³⁰⁻³⁴ and handedness selectivity.^{35,36} Alignment of nanotubes along a preferred direction has also been achieved, but often with significant caveats or over a limited scope. Researchers have used a variety of techniques to align nanotubes including non-chiral-enriched, vertically-oriented SWCNT forests,^{37,38} me-

chanical pulling of polymers,³⁹ solution-phase shearing,⁴⁰ electrostatic-enhanced dropcast films,⁴¹ magnetic alignment,⁴² nanowire self assembly,⁴³ and feedstock-driven growth.^{19,44} Recently, a significant step forward in SWCNT alignment was taken when He et al.^{45,46} demonstrated that SWCNTs formed along a particular axis when a nanotube solution was slowly filtered through a hydrophilic, polyvinylpyrrolidone (PVP)-coated nanoporous membrane. This observation has allowed researchers to produce well-aligned polarized SWCNT films *after* solution-based chemical processing (e.g., chiral enrichment or length sorting).^{7,8,12,47-49} Unfortunately, this technique is challenging to reproduce, difficult to scale up, and labor intensive, all of which has hindered the widespread adoption of this method. Furthermore, previous work on filtration-based nanotube alignment has claimed that these films are globally aligned, a statement challenged by the absence of a true macroscopic characterization technique, as well as a complete reliance on single-side film measurements.

In this Letter, we use an automated and parallelized filtration system to reproducibly and simultaneously create multiple highly-aligned, solution-based SWCNT films, thus allowing us to explore a large set of chemical and physical parameters under well-controlled conditions. Using machine vision, we both measure and control the filtration flow rate for different filter membrane pore sizes by monitoring the solution meniscus and regulating the transmembrane pressure. This automated feedback loop produces a constant filtration flow rate, which not only improves SWCNT alignment, but also enables this technique to be easily applied to different varieties of synthesized SWCNTs. Additionally, we use a combination of polarized optical techniques and glass silanation to discover and remove the formation of a meniscus-created radial SWCNT alignment. Spatial mapping of both sides of the SWCNT film using polarized Raman scattering shows a two-dimensional nematic ordering parameter, S_{2D} , of ≈ 0.9 throughout the film. This uniform value of S_{2D} unambiguously demonstrates true global alignment from solution-based SWCNTs. Fi-

nally, based on experiments tuning the electrostatic environment, we propose that charge ordering on the filter membrane is one of the driving forces involved in the spontaneous alignment of SWCNTs along a common axis.

To prepare our individualized SWCNT solution for filtration, we use Carbon Solutions (Riverside, CA) P2 arc-discharge SWCNTs (lot# 02-A011), which are dispersed via tip sonication⁵⁰ in 20 g/L sodium deoxycholate (DOC) in H₂O and then centrifuged to remove non-SWCNT contaminants. To mitigate discrepancies between water- and non-water-filled SWCNTs, we used nanotubes filled with C₇H₁₆.³⁴ Benefits of alkane-filled SWCNTs, including sharper optical features and a clear path towards alignment of confined molecules, are discussed in more detail in Campo et al.³⁴ and in the Supplementary Information. Additionally, the success of generating aligned SWCNT films (*vide infra*) with controlled filling presents a clear path for the alignment of confined molecules, which is of great interest for future efforts. Finally, a rate-zonal centrifugation method is applied to sort the nanotube solution to remove bent and very short SWCNTs. At the end of this multi-step procedure,³² which also includes removal of solution components other than H₂O, DOC, and SWCNTs via ultrafiltration and increasing the SWCNT concentration, we have a mixed-chirality SWCNT solution composed of long, straight tubes, in 10 g/L DOC, which are ideal for this alignment technique. Before filtration, the SWCNT dispersion is diluted to have a DOC concentration of 0.03 wt.% and an approximate SWCNT concentration of 8 $\mu\text{g}/\text{mL}$, which was determined through optical density measurements.

To automate the filtration setup shown in Figure 1a, we developed software to detect, numerically fit, and control the edge of the SWCNT solution meniscus. Meniscus detection and tracking was performed using an adaptable detection algorithm to convert the real image to an edge outline, as shown in Figure 1b. We developed software to numerically fit the meniscus edge from this outline, which significantly reduced fluctuation-created noise in the extraction process. Because the meniscus is tracked

as a function of time, it serves as a measure of flow rate. Pressure is maintained via a PID-controlled variable leak using a proportioning solenoid valve with an applied source vacuum of 28.8 kPa. Accurate and precise (± 2 Pa) applied pressure control is achieved across a broad pressure range of over four orders of magnitude from 3 Pa to 6000 Pa. The pressure is increased at the end of the filtration process to dry the film and prevent disruption of the still-wet SWCNT structure.

Besides eliminating human control from the alignment process, our machine vision-based SWCNT film configuration easily allows for production upscaling. As detailed in Figure 1a, although just one filtration rig ('master') is monitored, multiple films are simultaneously produced by putting filtration assemblies in parallel. Since each parallelized assembly is nearly identical to the master rig, excellent alignment for several SWCNT films is achieved. As an example of this high degree of uniformity achieved by our system, we show in Figure 1c three films simultaneously produced in our parallelized system that have nearly identical 2D nematic ordering. To numerically describe nematicity in our films, we use S_{2D} , which varies from 1 (perfect alignment) to -1 (exactly orthogonal), throughout this work (measurement details described below, in Figures S1 and S2, and the corresponding Supplementary Information text).

Figures 1d and 1e show that the SWCNT films are 178 ± 11 nm thick (in this paper, uncertainty is reported as $k = 1$ standard deviation), which is on the order of the length of one nanotube (≈ 200 nm to 400 nm). Because all of the films were made with the same SWCNT dispersion, nominal SWCNT concentration, and filtration assembly, we expect that the thicknesses of all the films to be similar to the one shown in Figure 1e. Nanotube film thicknesses on this order (and smaller) are often treated as 2D constructs, because of the dimensionality of their measured physical properties.⁵¹ We note that the film thicknesses measured here are on the high end of the thickness spectrum compared to those reported by prior groups,^{45,48} thus supporting our claim of excellent global

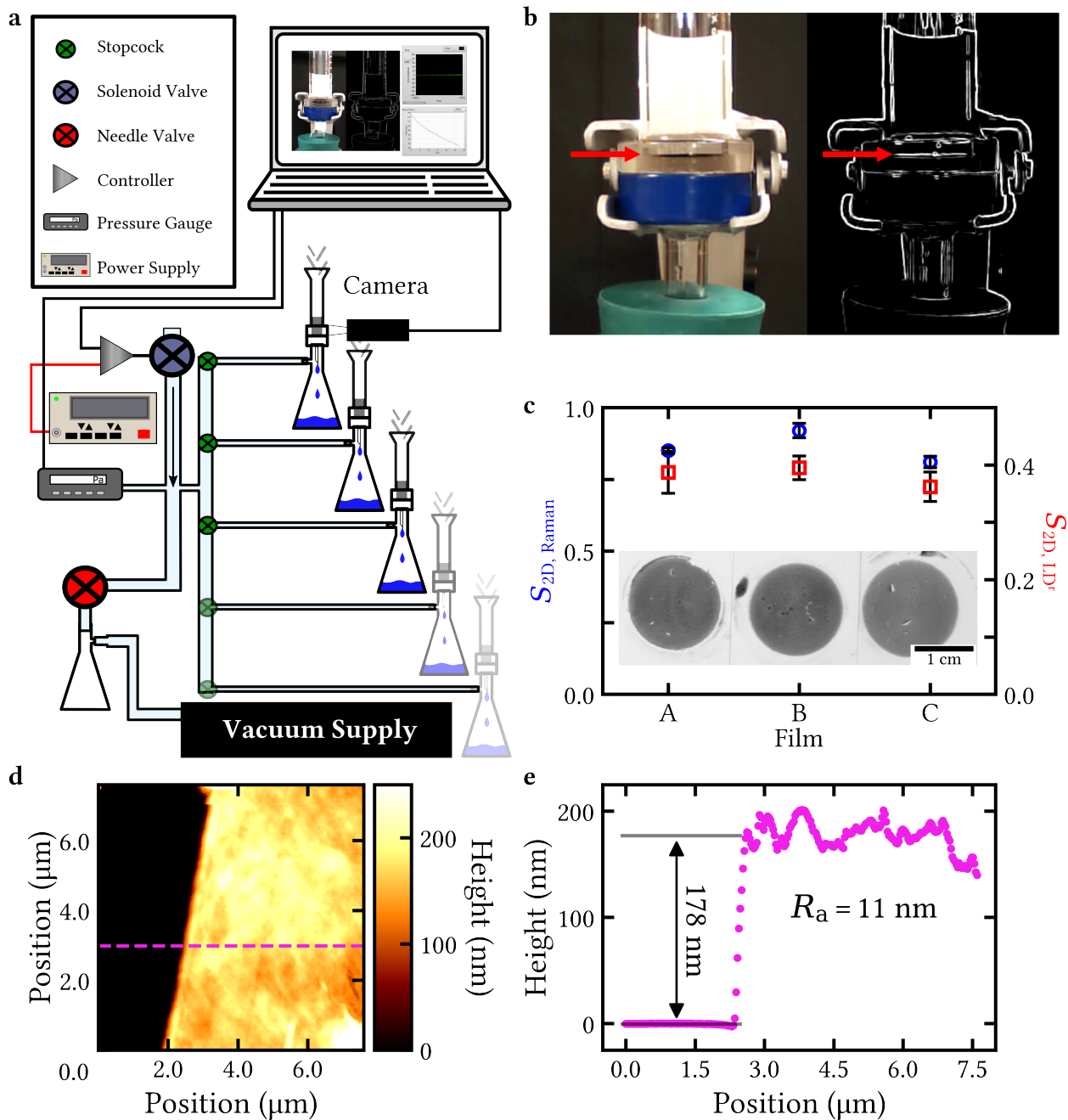


Figure 1. (a) Schematic of the automated, parallelized filtration assembly. The ability to simultaneously create multiple aligned SWCNT films using machine vision and a feedback-control system enables reproducible and scalable production. (b) (left) Image of the filtration assembly taken by the camera during filtration. (right) Corresponding contrast-enhanced edge image produced using the Canny edge algorithm. The arrows in both figures highlight the meniscus edge, which we detect, numerically fit, and monitor during filtration. (c) S_{2D} measurements of three films made in parallel using polarized Raman scattering (blue; left vertical axis) and reduced linear dichroism, LD_{2D}^F (red; right vertical axis). The high and uniform degree of alignment confirms that each separate arm of the parallelized system is equivalent. Depending on the measurement technique used, the measured value of S_{2D} on the same film varies substantially. Inset: pictures of the corresponding aligned SWCNT films. (d) Atomic force microscopy (AFM) height map of film made with 0.03 wt.% DOC. (e) AFM height profile extracted from the magenta line on (d). Measured film thickness of 178 ± 11 nm is on the order of one nanotube length. From the AFM film profile, a surface roughness, R_a , of 11 nm is obtained.

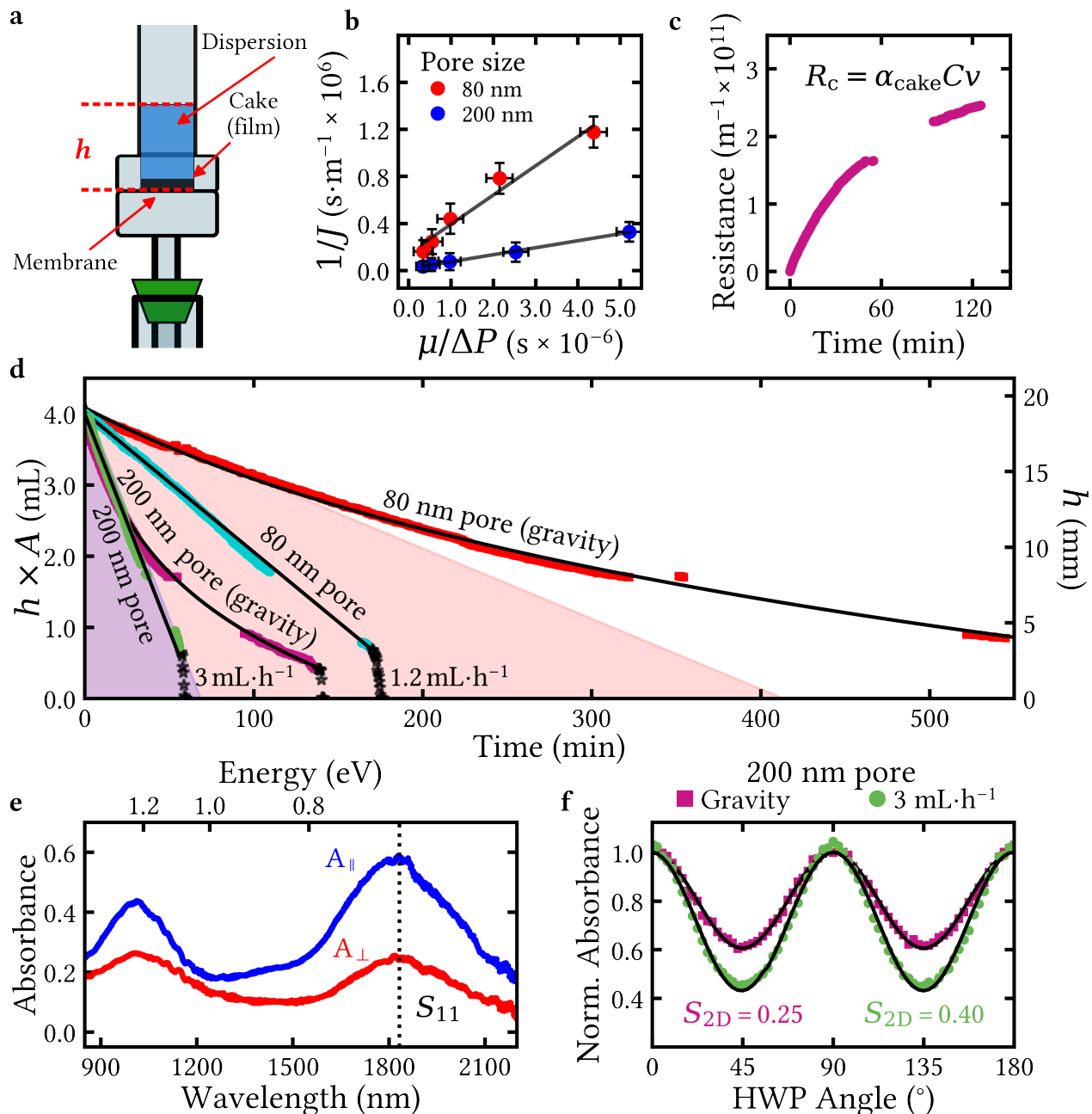


Figure 2. (a) Graphical depiction of the filtration setup. The height of the SWCNT dispersion, $h(t)$, is measured as a function of time, t , by a computer-monitored camera. (b) Reciprocal of the permeation flux, J , as a function of $\mu/\Delta P$ for the 80 nm (red) and 200 nm (blue) pore size membranes. The measured membrane resistance, R_m , is equal to $2.5 \times 10^{11} \text{ m}^{-1}$ for the 80 nm pore size membrane and $3.8 \times 10^{10} \text{ m}^{-1}$ for the 200 nm one. (c) Cake (i.e., the SWCNT film during filtration) resistance, R_c , as a function of time. As more SWCNTs are deposited on the membrane surface, the overall resistance to flow increases. Data shown for a 80 nm pore size membrane and a SWCNT concentration of $8 \mu\text{g}/\text{mL}$. (d) Time-dependence of the measured SWCNT dispersion volume for different filter pore sizes and pressure conditions. The gravity filtration data and fit (black curve) denote the flow rate lower limit that is possible with a given membrane pore size. The shaded regions for both the 80 nm (pink) and 200 nm (purple) membrane pore sizes indicate the accessible region of achievable flow rates that can be obtained using the results from (b) and (c). Gaps in the data are created when the meniscus goes behind the glass funnel lip. Starred points denote the film drying process, where the pressure is increased. (e) Polarized absorbance spectra of a SWCNT film produced using the 200 nm pore membrane. A half-wave plate (HWP) rotates the light polarization with respect to the alignment direction. The black dashed line indicates the S_{11} absorbance feature at 1818 nm of one of the nanotube chiralities. (f) Normalized polarized S_{11} absorption of a film made with the 200 nm pore membrane using a constant flow rate (green) and gravity filtration (purple).

alignment over a substantial SWCNT deposition amount.

The combination of automation and parallelization enables us to produce multiple copies of aligned films under a wide range of different physical and chemical conditions. Previous SWCNT alignment protocols have been unable to achieve a constant filtration flow rate, which results in a time-varying SWCNT cake (i.e., film during filtration) deposition rate, thus hindering optimal SWCNT alignment. In order to achieve a constant filtration flow rate, which is expressed as a permeation flux, J ($= \frac{\text{flow rate}}{\text{area}}$), we first had to empirically determine the membrane resistance, R_m , and cake resistance, R_c :

$$\frac{1}{J} = \frac{\mu(R_m + R_c)}{\Delta P}, \quad (1)$$

where μ is the viscosity of the permeate (SWCNT solution), ΔP is transmembrane pressure, and $R_c = \alpha_{\text{cake}} C v$ with α_{cake} as the specific cake resistance, C the dispersion concentration, and v the filtrate volume per unit area (see Figure S3 for information about the measurement of α_{cake}). R_m , which is independently measured through a controlled water filtration experiment shown in Figure 2b, is $2.5 \times 10^{11} \text{ m}^{-1}$ for the 80 nm pore-size membrane and $3.8 \times 10^{10} \text{ m}^{-1}$ for the 200 nm pore-size membrane. While R_m is nearly constant throughout the filtration process, R_c increases with time as the cake is deposited, which is shown in Figure 2c. Using our determination of the time-independent R_m and the time-dependent R_c , we can then tune ΔP throughout the film deposition to keep J constant. It should be noted that ΔP is the total (time-dependent) transmembrane pressure, which is the sum of the applied pressure, P_{applied} , and the head pressure, $\rho g h(t)$, where ρ is the dispersion mass density, g is gravitational acceleration, and $h(t)$ is the time-dependent solution column height.

Figure 2d shows our ability to achieve a constant flow rate for two membrane pore sizes (80 nm, cyan trace; and 200 nm, green trace) throughout the entire film deposition process. Gravity-driven filtration (i.e., no applied pressure; red and purple traces) curves demarcate

the slowest flow rate possible in our system with a specific R_m , while the colored regions (pink and purple for 80 nm and 200 nm pore-size membranes, respectively) indicate the possible range of flows accessible when external pressure is applied (see Figure S4 for a more-detailed view of Figure 2d). The high value of R_m for the 80 nm pore-size membrane allows for a greater variability of the flow rate, but often at lower values of J . Critically, the procedure that we delineate here, measuring R_m and R_c and then tuning ΔP to maintain a constant J , paves the way to apply this method to different SWCNT types (laser oven, HiPCO, CoMoCAT, arc discharge, etc.) and membranes with differing pore sizes and materials. As an example of this utility, we report on the measured α_{cake} for CoMoCAT SWCNTs in the Supplementary Information. Thus, our procedure greatly broadens the applicability and utility of this filtration-based alignment method.

Throughout this Letter, we use several optical spectroscopic techniques to determine S_{2D} for our SWCNT films after they have been transferred to either a glass coverslip or quartz substrate (see Figure S5 for details regarding the film transfer). Since SWCNTs have a highly anisotropic absorption coefficient, α , polarized optical spectroscopic techniques are commonly used to measure nematicity in SWCNTs. In this work, we rely on three polarized optical methods to determine nematicity: polarized Raman scattering (Figure S1), reduced linear dichroism, LD_{2D}^r , and birefringence ratios (Figure S2; precise formulations are given in the Supplementary Information). The guiding principle behind all three methods is graphically captured by Figure 2e, which shows that when the optical electric field is parallel to the SWCNT axis, the on-axis absorption coefficient, α_{\parallel} , is high; in contrast, when the electric field is orthogonal to the SWCNT axis, the off-axis absorption coefficient, α_{\perp} , is suppressed. Depending on the optical technique, we either rotate the light polarization angle using a half-wave plate (HWP), or keep the light polarization fixed and rotate the SWCNT film; in both cases, α_{\parallel} and α_{\perp} are probed.

The anisotropic SWCNT absorption provides

a way to measure S_{2D} , which as mentioned above, is our metric for determining alignment. To relate S_{2D} to polarized Raman scattering measurements, we use a combination of polarization-specific geometries with respect to the vertically-oriented SWCNT absorption axis:⁵²

$$S_{2D} = \frac{\Delta I_{VV} - I_{HH}}{\Delta I_{VV} + I_{HH} + (1 + \Delta)I_{VH}}, \quad (2)$$

where I_{XY} is measured scattering intensity with the incident (X) and scattered (Y) light polarization oriented vertically (V ; parallel to the SWCNT axis) or horizontally (H ; perpendicular to the SWCNT axis) and Δ is the dichroic ratio $\Delta = \frac{\alpha_{\parallel}}{\alpha_{\perp}}$. We can also use reduced linear dichroism, LD_{2D}^r , an strictly absorption-based technique, to measure S_{2D} :⁴⁹

$$S_{2D} = \frac{LD_{2D}^r}{2} = \frac{(\alpha_{\parallel} - \alpha_{\perp})}{\alpha_{\parallel} + \alpha_{\perp}}. \quad (3)$$

In the ideal scenario, all empirical methods for determining S_{2D} convergence on the same value. However, in reality, the measurement method strongly affects the value of S_{2D} in SWCNTs. In particular, S_{2D} measured via optical absorption-based methods, such as LD_{2D}^r , is likely to *significantly* underestimate SWCNT alignment due to wavelength-dependent features, such as non-excitonic absorption and cross-polarized optical transitions.^{49,53} Although absorption-based measurements of S_{2D} are still valuable, especially for relative comparisons, the alignment values obtained from these techniques represent the minimal degree of SWCNT film alignment averaged over a millimeter-sized area. This disparity in S_{2D} measured using different techniques (polarized Raman scattering and LD_{2D}^r) is clearly shown in Figure 1c. Given the significantly reduced effect of non-axial SWCNT spectroscopic features, we use polarized Raman to determine S_{2D} when possible. We note that excellent work using terahertz spectroscopy^{17,45} to determine nanotube alignment is another background-less technique that achieves highly accurate values of nematicity.

Figure 2f compares the LD_{2D}^r of films made

via gravity-driven filtration (purple) and using a constant flow rate filtration (green). Although the S_{11} absorption used to calculate LD_{2D}^r underestimates the true value of S_{2D} as discussed earlier, it is very clear from this figure that greater alignment (i.e., a higher LD_{2D}^r value) is achieved when the flow rate is fixed. Thus, although optimization was not a goal of this work, flow rate control improves reproducibility and nematicity. Furthermore, when the filtration parameters of a SWCNT dispersion and nanoporous membrane have been determined, precise flow rate control is fully generalizable to other SWCNT populations.

Along with flow rate control, we also detect and address a previously unreported effect in SWCNT films created by the meniscus of the SWCNT dispersion during filtration. Specifically, our use of spatially-resolved polarized optical techniques, such as birefringence and polarized Raman scattering mapping, reveals the presence of a *radial* SWCNT alignment on the front surface of our films (i.e., the side that faces upward during filtration). This type of alignment (at least in three dimensions) is known as a spherulite and is commonly observed in films of 1D crystals when the solution meniscus combs (or drags) across the film surface, which produces a force director that radially polarizes the crystals (Figure 3c). As Figures 3a and 3d clearly indicate, we observe this radial alignment on the surface of our SWCNT films due to meniscus combing during the final stages of our filtration; we refer to this feature as a 2D spherulite. To remove this meniscus-created radial orientation, we increased the hydrophobicity of our filtration glassware using a silanation procedure (see Figure S6 and the associated text in the Supplementary Information for details). This technique greatly flattens the meniscus and prevents it from dragging across the SWCNT cake at the end of filtration (Figure 3c). Figures 3b and 3e show the results of flat-meniscus filtration. In stark contrast to the traditional SWCNT alignment method, the nanotubes on *both* sides of the film in Figure 3e are well ordered (see Figures S7 and S8 for Raman maps of both front and back

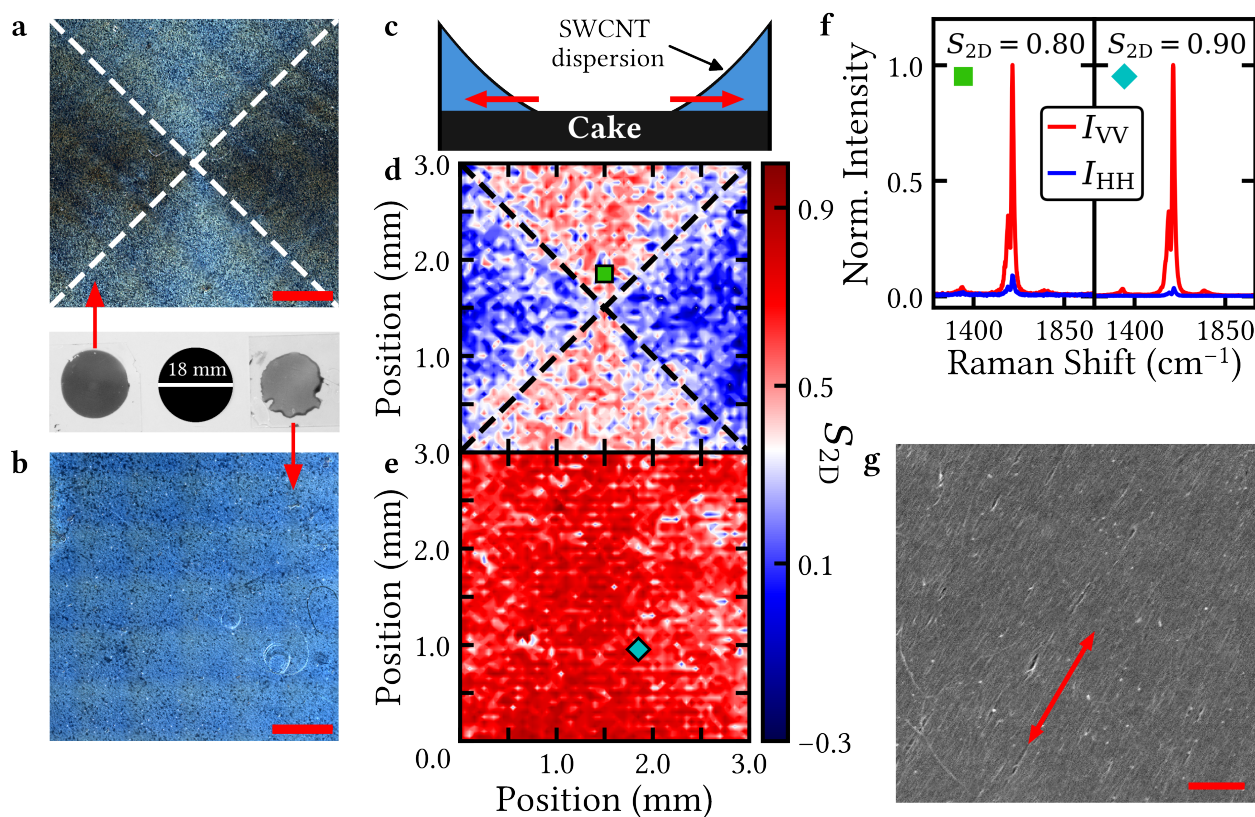


Figure 3. (a) Cross-polarized microscope image showing the formation of a 2D spherulite (radial surface SWCNT alignment due to meniscus combing) on the front side of the SWCNT film. Scale bar: $1500 \mu\text{m}$. (b) Cross-polarized microscope image of a SWCNT film created using silanated glassware, a procedure which significantly flattens the meniscus. Despite imaging over a large area of the film, there are no signs of a 2D spherulite. Scale bar: $1500 \mu\text{m}$. (c) Radial alignment of the SWCNTs (and uneven cake deposition) is created by meniscus combing at the end of the filtration process. The red arrows indicate the radially aligned force director at the cake surface. (d) Spatial map of S_{2D} of the front side of the film in (a) as measured by polarized Raman spectroscopy at 532 nm . The formation a radial pattern and a lack of global alignment across the front surface of the SWCNT film is clearly observed. The square marker indicates where the Raman spectrum shown in (f) is taken. (e) Spatial map of S_{2D} for the front side of the film in (b). The high degree of SWCNT alignment over a large area and distinct lack of a 2D spherulite formation provide strong evidence that the meniscus flattening eliminates SWCNT radial polarization. The diamond marker indicates where the Raman spectrum shown (f) is taken. (f) Polarized Raman spectra of films in (a) (left) and (b) (right). The red traces (I_{VV}) are measured with the incident and scattered light both polarized along the SWCNT film axis, while the blue traces (I_{HH}) are measured with the incident and scattered light polarized perpendicular to this axis. These measurements are necessary for calculating S_{2D} . (g) Scanning electron microscopy image of a SWCNT film made with $0.03 \text{ wt.}\%$ DOC. Arrow indicates alignment axis. Scale bar: 500 nm .

film surfaces). Importantly, this double-sided alignment extends across large distances, which demonstrates global SWCNT nematic ordering.

Interestingly, depending on the thickness of the film, the skin depth of the optical probe, and whether the probe measures reflection or transmission, the use of polarized optical spectroscopy may not unambiguously detect the presence of a 2D spherulite. This point is strengthened when one remembers that after the film is transferred from the membrane to a substrate, the front film surface during filtration is now the back film surface for optical measurements, which may not always be as well measured as the front surface. Figures 3f and S7c capture the non-obvious signature of the 2D spherulite behavior: although S_{2D} is clearly increased when the 2D spherulite is removed through silanating the glassware, the effect on the measured nematicity is not huge. Only through the careful spatial mapping of *both* SWCNT film surfaces does the radial polarization, and thus lack of global ordering, appear. The high degree of alignment across the non-spherulite film is additionally supported through direct imaging techniques like scanning electron microscopy (Figure 3g), which clearly indicates excellent SWCNT alignment.

We also investigated the SWCNT alignment mechanism using our automated filtration system with the previously described improvements to the alignment protocol. Figure 4a shows grooves in the filter membrane created during the manufacturing process. Although these grooves are not uniformly spaced or appropriately sized for the nanotubes we are using, they still raise an important question about whether or not they play a role in nanotube alignment. To help address what part, if any, these channels play in nanotube alignment, we augment the grooving by sweeping an ethanol-wetted wipe across the top surface of the filter membrane along the initial groove direction (Figure 4b) prior to filtration. We compared the resulting SWCNT film to one made with a filter membrane swept with a water-wetted wipe to attempt to keep the mechanical grooving the same in both cases. As shown in Figure S9, the ethanol-wiped filter membrane increases

the SWCNT film alignment considerably going from a LD_{2D}^* -determined S_{2D} of 0.26 to 0.42. In contrast, the film made with the water-wiped membrane had nearly an identical S_{2D} ($= 0.27$) as the SWCNT film made without any filter pretreatment. This ethanol-wiped enhancement strongly suggests that ordered charging, instead of mechanical grooving, is responsible for increased SWCNT alignment. We note that a similar increase in SWCNT alignment was observed in self-assembled SWCNT nanowires when the glass substrates were directionally wiped with ethanol.⁴³

Along with charging the membrane, inter-SWCNT electrostatic interactions are another significant factor determining S_{2D} . As shown previously,⁴⁵ the DOC concentration of the SWCNT solution strongly impacts the achievable S_{2D} (Figure 4c). This observation may be due to a decreased Debye length electrostatic interaction scale between (1) individualized SWCNTs and (2) SWCNTs and the membrane, as the DOC concentration is increased. Additionally, there may be a role played by an (assumed) increase in the coverage of nanotubes by surfactant molecules that occurs with larger DOC concentrations. The measured S_{2D} scaling with DOC concentration strongly guided our decision to use solutions with 0.03 wt.% DOC concentration, which is over an order of magnitude below the critical micelle concentration.^{54,55} Further experiments using NaCl to tune the ionic strength confirm that as the tube-tube electrostatic interactions decrease due to increased screening, the SWCNT nematicity plummets (Figure 4d).

The strong role played by directional charging and inter-tube electrostatics suggests that the Debye length effect discussed earlier likely dominates: that is, the director field for SWCNT alignment is very likely transmitted via electrostatic interactions. Although mechanical membranes grooves may play a minor role in nanotube alignment, the large size of the grooves, lack of groove uniformity, and their relative irregularity all suggest that they are not directly responsible for SWCNT alignment. Instead, one hypothesis that fits our observations is that linear arrays of charge are formed on

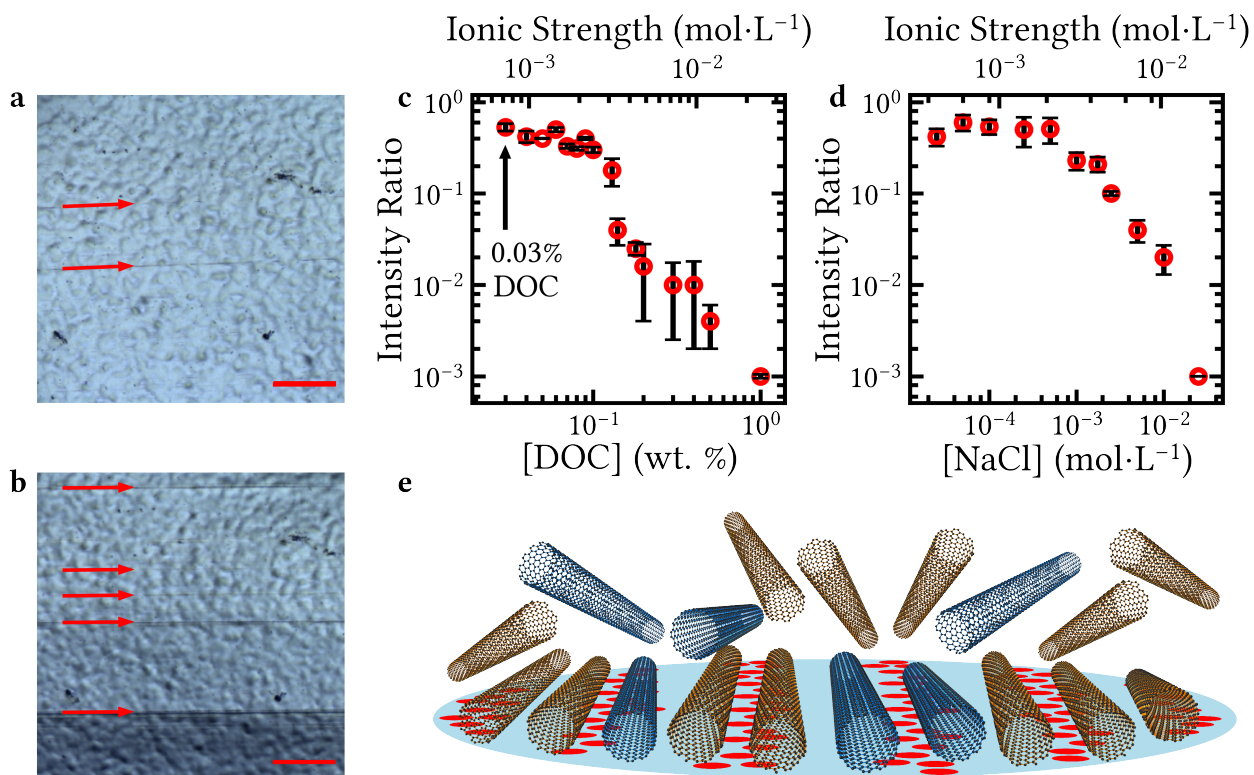


Figure 4. (a) Microscope image of a membrane used for the filtration process. Small grooves (indicated by the red arrows) are observed on the surface, which are created from the membrane production process. Scale bar: 250 μm . (b) Although groove density is increased when the membrane PVP surface in (a) is swept with ethanol-wetted wipe, we find that the grooving is not as important as charging. Scale bar: 250 μm . As the concentration of (c) DOC and (d) NaCl increases (i.e., inter-SWCNT electrostatic interactions decrease), the birefringence intensity ratio of the SWCNT film is sharply depressed. These behaviors confirm that the inter-nanotube electrostatic environment is critical to the formation of aligned SWCNT films. For clarity, representative error bars are shown for five points. (e) Graphical depiction of our proposed model for ordered SWCNT formation. Charges puddle on the filtration membrane in quasi-linear chains created by intentional wiping. These electrostatic fields, in competition with the complex electrostatic inter-nanotube environment, compete to produce an aligned SWCNT phase on the membrane.

the filter membrane, as depicted in Figure 4e. It is unclear whether these charges would be caused by physically aligning (charged) PVP polymers, directionally tribocharging the membrane, or a combination of both.^{56–60} Regarding the polymer orientation hypothesis, the mechanical processing of the filter membranes, which creates the observed grooving in Figure 4, very likely has the additional property of aligning the (charged or easily ionized) PVP polymer molecules that make up the membrane coating. When charged, these linearly-oriented molecules would then produce SWCNT alignment along a common axis that coincides with the grooves. The phenomenon of directional charging has been observed in a host of situations by numerous researchers, including efforts to pattern surface charges^{58,61} and to align particles via electrostatic puddling.⁶² Similar alignment behavior is also observed with substrate “buffing” for liquid crystals and polymer substrates.^{56,57,63,64} Despite the well-known existence of an electrostatically created director field, the actual mechanism behind the effectiveness of buffing is still in dispute and is believed to vary with the substrate type. Further work on how to enhance and control charge araying on filter membranes is ongoing.

In summary, we have created an automated, parallelized SWCNT filtration system that can create simultaneous and reproducible SWCNT films with a high degree of true global alignment. We find that holding the filtration flow rate constant using our pressure-controlled system enhances the nematic order of our films. In addition, we both measure and remove 2D spherulite formation on the front-surface of the SWCNT films by flattening the meniscus using silanated glassware. We propose that directional charging on the filter membrane and inter-SWCNT electrostatic interactions are the two driving forces behind the alignment of nanotubes using this filtration technique. Our innovations on the SWCNT filtration method, as well as the results described here, pave a clear path for both research- and industrial-scale implementation of highly aligned SWCNT films from aqueous solutions.

Acknowledgement The authors thank Dr. Joseph R. Murphy for his input on the machine-vision implementation and AFM data processing, and Dr. John Ackerman for his help with the glassware silanation. TAS acknowledges funding from the W. M. Keck Foundation, and JSW and WDR acknowledge funding from the School of Energy Resources at the Univ. of WY.

Supporting Information Available: This material is available free of charge via the Internet at <http://pubs.acs.org/>.

Corresponding Author

*wrice2@uwyo.edu

Notes

The authors declare no competing financial interest.

References

- (1) Voit, J. One-dimensional Fermi liquids. *Rep. Prog. Phys.* **1995**, *58*, 977.
- (2) Bockrath, M.; Cobden, D. H.; Lu, J.; Rinzler, A. G.; Smalley, R. E.; Balents, L.; McEuen, P. L. Luttinger-liquid behavior in carbon nanotubes. *Nature* **1999**, *397*, 598–601.
- (3) Shi, Z.; Hong, X.; Bechtel, H. A.; Zeng, B.; Martin, M. C.; Watanabe, K.; Taniguchi, T.; Shen, Y.-R.; Wang, F. Observation of a Luttinger-liquid plasmon in metallic single-walled carbon nanotubes. *Nature Photonics* **2015**, *9*, 515.
- (4) Fidkowski, L.; Kitaev, A. Effects of interactions on the topological classification of free fermion systems. *Phys. Rev. B* **2010**, *81*, 134509.
- (5) Fidkowski, L.; Kitaev, A. Topological phases of fermions in one dimension. *Phys. Rev. B* **2011**, *83*, 075103.
- (6) Deshpande, V. V.; Bockrath, M. The one-dimensional Wigner crystal in carbon nanotubes. *Nature Phys.* **2008**, *4*, 314.

- (7) Gao, W.; Li, X.; Bamba, M.; Kono, J. Continuous transition between weak and ultrastrong coupling through exceptional points in carbon nanotube microcavity exciton-polaritons. *Nature Photonics* **2018**, *12*, 362.
- (8) Ho, P.-H.; Farmer, D. B.; Tulevski, G. S.; Han, S.-J.; Bishop, D. M.; Gignac, L. M.; Bucchignano, J.; Avouris, P.; Falk, A. L. Intrinsically ultrastrong plasmon-exciton interactions in crystallized films of carbon nanotubes. *Proc. Natl. Acad. Sci. USA* **2018**, *115*, 12662.
- (9) Torres, J.; Coquillat, D.; Legros, R.; Lascaray, J. P.; Teppe, F.; Scalbert, D.; Peyrade, D.; Chen, Y.; Briot, O.; d'Yerville, M. L. V.; Centeno, E.; Casagne, D.; Albert, J. P. Giant second-harmonic generation in a one-dimensional GaN photonic crystal. *Phys. Rev. B* **2004**, *69*, 085105.
- (10) Ajiki, H.; Ando, T. Aharonov-Bohm effect in carbon nanotubes. *Physica B: Condensed Matter* **1994**, *201*, 349.
- (11) Zaric, S.; Ostojic, G. N.; Kono, J.; Shaver, J.; Moore, V. C.; Strano, M. S.; Hauge, R. H.; Smalley, R. E.; Wei, X. Optical signatures of the Aharonov-Bohm phase in single-walled carbon nanotubes. *Science* **2004**, *304*, 1129.
- (12) Yanagi, K.; Okada, R.; Ichinose, Y.; Yomogida, Y.; Katsutani, F.; Gao, W.; Kono, J. Intersubband plasmons in the quantum limit in gated and aligned carbon nanotubes. *Nature Comm.* **2018**, *9*, 1121.
- (13) Autés, G. et al. A novel quasi-one-dimensional topological insulator in bismuth iodide β -Bi₄I₄. *Nature Mater.* **2016**, *15*, 154.
- (14) Yao, Z.; Kane, C. L.; Dekker, C. High-Field Electrical Transport in Single-Wall Carbon Nanotubes. *Phys. Rev. Lett.* **2000**, *84*, 2941–2944.
- (15) Huang, J.-W.; Pan, C.; Tran, S.; Cheng, B.; Watanabe, K.; Taniguchi, T.; Lau, C. N.; Bockrath, M. Superior current carrying capacity of boron nitride encapsulated carbon nanotubes with zero-dimensional contacts. *Nano Lett.* **2015**, *15*, 6836.
- (16) Harnack, O.; Pacholski, C.; Weller, H.; Yasuda, A.; Wessels, J. M. Rectifying behavior of electrically aligned ZnO nanorods. *Nano Lett.* **2003**, *3*, 1097.
- (17) Ren, L.; Pint, C. L.; Booshehri, L. G.; Rice, W. D.; Wang, X.; Hilton, D. J.; Takeya, K.; Kawayama, I.; Tonouchi, M.; Hauge, R. H.; Kono, J. Carbon Nanotube Terahertz Polarizer. *Nano Lett.* **2009**, *9*, 2610.
- (18) He, X.; Fujimura, N.; Lloyd, J. M.; Erickson, K. J.; Talin, A. A.; Zhang, Q.; Gao, W.; Jiang, Q.; Kawano, Y.; Hauge, R. H.; Léonard, F.; Kono, J. Carbon nanotube terahertz detector. *Nano Lett.* **2014**, *14*, 3953.
- (19) Cubukcu, E.; Degirmenci, F.; Kocabas, C.; Zimmler, M. A.; Rogers, J. A.; Capasso, F. Aligned carbon nanotubes as polarization-sensitive, molecular near-field detectors. *Proc. Natl. Acad. Sci. USA* **2009**, *106*, 2495.
- (20) Wei, W.; Wang, Y.; Ji, J.; Zuo, S.; Li, W.; Bai, F.; Fan, H. Fabrication of large-area arrays of vertically aligned gold nanorods. *Nano Lett.* **2018**, *18*, 4467.
- (21) Chen, P.; Fu, Y.; Aminirad, R.; Wang, C.; Zhang, J.; Wang, K.; Galatsis, K.; Zhou, C. Fully printed separated carbon nanotube thin film transistor circuits and its application in organic light emitting diode control. *Nano Lett.* **2011**, *11*, 5301.
- (22) Green, M. E.; Bas, D. A.; Yao, H.-Y.; Gengler, J. J.; Headrick, R. J.; Back, T. C.; Urbas, A. M.; Pasquali, M.; Kono, J.; Her, T.-H. Bright and Ultrafast Photoelectron Emission from Aligned Single-

- Wall Carbon Nanotubes through Multi-photon Exciton Resonance. *Nano Lett.* **2019**, *19*, 158.
- (23) Zhang, Q.; Liu, C.; Liu, X.; Liu, J.; Cui, Z.; Zhang, Y.; Yang, L.; Zhao, Y.; Xu, T. T.; Chen, Y.; Wei, J.; Mao, Z.; Li, D. Thermal transport in quasi-1D van der Waals crystal Ta₂Pd₃Se₈ nanowires: size and length dependence. *ACS Nano* **2018**, *12*, 2634.
- (24) Nanot, S.; Thompson, N. A.; Kim, J.-H.; Wang, X.; Rice, W. D.; H roz, E. H.; Ganesan, Y.; Pint, C. L.; Kono, J. In *Springer Handbook of Nanomaterials*; Vajtai, R., Ed.; Springer-Verlag: Berlin Heidelberg, 2013; Chapter Single-Walled Carbon Nanotubes.
- (25) Zheng, M. Sorting carbon nanotubes. *Top. Curr. Chem.* **2017**, *375*, 13.
- (26) Bati, A. S. R.; Yu, L.; Batmunkh, M.; Shapter, J. G. Synthesis, purification, properties and characterization of sorted single-walled carbon nanotubes. *Nanoscale* **2018**, *10*, 22087.
- (27) Janas, D. Towards monochiral carbon nanotubes: a review of progress in the sorting of single-walled carbon nanotubes. *Mater. Chem. Front.* **2018**, *2*, 36.
- (28) Fagan, J. Aqueous two-polymer phase extraction of single-wall carbon nanotubes using surfactants. *Nanoscale Adv.* **2019**,
- (29) Khripin, C. Y.; Tu, X.; Heddleston, J. M.; Silvera-Batista, C.; Walker, A. R. H.; Fagan, J.; Zheng, M. High-resolution length fractionation of surfactant-dispersed carbon nanotubes. *Anal. Chem.* **2013**, *85*, 1382.
- (30) Takenobu, T.; Takano, T.; Shiraishi, M.; Murakami, Y.; Ata, M.; Kataura, H.; Achiba, Y.; Iwasa, Y. Stable and controlled amphoteric doping by encapsulation of organic molecules inside carbon nanotubes. *Nature Mater.* **2003**, *2*, 683.
- (31) Cambr , S.; Wenseleers, W. Separation and diameter sorting of empty (end-capped) and water-filled (open) carbon nanotubes by density gradient ultracentrifugation. *Angew. Chem. Intl. Ed.* **2011**, *50*, 2764.
- (32) Fagan, J. A.; Huh, J. Y.; Simpson, J. R.; Blackburn, J. L.; Holt, J. M.; Larsen, B. A.; Walker, A. R. H. Separation of empty and water-filled single-wall carbon nanotubes. *ACS Nano* **2011**, *5*, 3943.
- (33) Cambr , S.; Campo, J.; Beirnaert, C.; Verlackt, C.; Cool, P.; Wenseleers, W. Asymmetric dyes align inside carbon nanotubes to yield a large nonlinear optical response. *Nature Nanotech.* **2015**, *10*, 248.
- (34) Campo, J.; Piao, Y.; Lam, S.; Stafford, C. M.; Streit, J. K.; Simpson, J. R.; Walker, A. R. H.; Fagan, J. A. Enhancing single-wall carbon nanotube properties through controlled endohedral filling. *Nanoscale Horizon* **2016**, *1*, 317.
- (35) Ao, G.; Streit, J. K.; Fagan, J. A.; Zheng, M. Differentiating left- and right-handed carbon nanotubes by DNA. *J. Am. Chem. Soc.* **2016**, *138*, 16677.
- (36) Wei, X.; Tanaka, T.; Yomogida, Y.; Sato, N.; Saito, R.; Kataura, H. Experimental determination of excitonic band structures of single-walled carbon nanotubes using circular dichroism spectra. *Nature Comm.* **2016**, *7*, 12899.
- (37) Hata, K.; Futaba, D. N.; Mizuno, K.; Namai, T.; Yumura, M.; Iijima, S. Water-assisted highly efficient synthesis of impurity-free single-walled carbon nanotubes. *Science* **2004**, *306*, 1362.
- (38) Murakami, Y.; Chiashi, S.; Miyauchi, Y.; Hu, M. H.; Ogura, M.; Okubo, T.; Maruyama, S. Growth of vertically aligned single-walled carbon nanotube films on quartz substrates and their optical anisotropy. *Chem. Phys. Lett.* **2004**, *385*, 298.

- (39) Jin, L.; Bower, C.; Zhou, O. Alignment of carbon nanotubes in a polymer matrix by mechanical stretching. *Appl. Phys. Lett.* **1998**, *73*, 1197.
- (40) Headrick, R. J.; Tsentelovich, D. E.; Berdegué, J.; Amram Bengio, E.; Liberman, L.; Kleinerman, O.; Lucas, M. S.; Talmon, Y.; Pasquali, M. Structure-property relations in carbon nanotube fibers by downscaling solution processing. *Adv. Mater.* **2018**, *30*, 1704482.
- (41) LeMieux, M. C.; Roberts, M.; Barman, S.; Jin, Y. W.; Kim, J. M.; Bao, Z. Self-sorted, aligned nanotube networks for thin-film transistors. *Science* **2008**, *321*, 101.
- (42) Walters, D. A.; Casavant, M. J.; Qin, X. C.; Huffman, C. B.; Boul, P. J.; Ericson, L. M.; Háróz, E. H.; O'Connell, M. J.; Smith, K.; Colbert, D. T.; Smalley, R. E. In-plane-aligned membranes of carbon nanotubes. *Chem. Phys. Lett.* **2001**, *338*, 14.
- (43) Hobbie, E. K.; Fagan, J. A.; Becker, M. L.; Hudson, S. D.; Fakhri, N.; Pasquali, M. Self-assembly of ordered nanowires in biological suspensions of single-wall carbon nanotubes. *ACS Nano* **2009**, *3*, 189.
- (44) Che, Y.; Wang, C.; Liu, J.; Liu, B.; Lin, X.; Parker, J.; Beasley, C.; Wong, H.-S. P.; Zhou, C. Selective synthesis and device applications of semiconducting single-walled carbon nanotubes using isopropyl alcohol as feedstock. *ACS Nano* **2012**, *6*, 7454.
- (45) He, X.; Gao, W.; Xie, L.; Li, B.; Zhang, Q.; Lei, S.; Robinson, J. M.; Háróz, E. H.; Doorn, S. K.; Vajtai, R.; Ajayan, P. M.; Adams, W. W.; Hauge, R. H.; Kono, J. Wafer-Scale Monodomain Films of Spontaneously Aligned Single-Walled Carbon Nanotubes. *Nature Nanotech.* **2016**, *11*, 633.
- (46) Gao, W.; Kono, J. Science and applications of wafer-scale crystalline carbon nanotube films prepared through controlled vacuum filtration. *R. Soc. open sci.* **2019**, *6*, 181605.
- (47) Komatsu, N.; Gao, W.; Chen, P.; Guo, C.; Babakhani, A.; Kono, J. Modulation-doped multiple quantum wells of aligned single-wall carbon nanotubes. *Adv. Funct. Mater.* **2017**, *27*, 1606022.
- (48) Chiu, K.-C.; Falk, A. L.; Ho, P.-H.; Farmer, D. B.; Tulevski, G.; Lee, Y.-H.; Avouris, P.; Han, S.-J. Strong and broadly tunable plasmon resonances in thick films of aligned carbon nanotubes. *Nano Lett.* **2017**, *17*, 5641.
- (49) Katsutani, F.; Gao, W.; Li, X.; Ichinose, Y.; Yomogida, Y.; Yanagi, K.; Kono, J. Direct observation of cross-polarized excitons in aligned single-chirality single-wall carbon nanotubes. *Phys. Rev. B* **2019**, *99*, 035426.
- (50) Certain equipment, instruments or materials are identified in this paper in order to adequately specify the experimental details. Such identification does not imply recommendation by the National Institute of Standards and Technology (NIST) nor does it imply the materials are necessarily the best available for the purpose.
- (51) Wang, X.; Gao, W.; Li, X.; Zhang, Q.; Nanot, S.; Háróz, E. H.; Kono, J.; Rice, W. D. Magnetotransport in type-enriched single-wall carbon nanotube networks. *Phys. Rev. Mater.* **2018**, *2*, 116001.
- (52) Zamora-Ledezma, C.; Blanc, C.; Maugey, M.; Zakri, C.; Poulin, P.; Anglaret, E. Anisotropic thin films of single-wall carbon nanotubes from aligned lyotropic nematic suspensions. *Nano Lett.* **2008**, *8*, 4103.
- (53) Kilina, S.; Tretiak, S.; Doorn, S. K.; Luo, Z.; Papadimitrakopoulos, F.; Piryatinski, A.; Saxena, A.; Bishop, A. R.

- Cross-polarized excitons in carbon nanotubes. *Proc. Natl. Acad. Sci. USA* **2008**, *105*, 6797.
- (54) Esposito, G.; Giglio, E.; Pavel, N. V.; Zanobi, A. Size and shape of sodium deoxycholate micellar aggregates. *J. Phys. Chem.* **1987**, *91*, 356.
- (55) D'Alagni, M.; D'Archivio, A. A.; Galantini, L.; Giglio, E. Structural study of the micellar aggregates of sodium chenodeoxycholate and sodium deoxycholate. *Langmuir* **1997**, *13*, 5811.
- (56) Toney, M. F.; Russell, T. P.; Anthony Logan, J.; Kikuchi, H.; Sands, J. M.; Kumar, S. K. Near-surface alignment of polymers in rubbed films. *Nature* **1995**, *374*, 709.
- (57) Hartmann, L.; Tremel, K.; Uttiya, S.; Crossland, E.; Ludwigs, S.; Kayunkid, N.; Vergnat, C.; Brinkmann, M. 2D versus 3D crystalline order in thin films of regioregular poly(3-hexylthiophene) oriented by mechanical rubbing and epitaxy. *Adv. Funct. Mater.* **2011**, *21*, 4047.
- (58) Burgo, T. A. L.; Ducati, T. R. D.; Francisco, K. R.; Clinckspoor, K. J.; Galembeck, F.; Galembeck, S. E. Triboelectricity: Macroscopic charge patterns formed by self-arraying ions on polymer surfaces. *Langmuir* **2012**, *28*, 7407.
- (59) Biniek, L.; Pouget, S.; Djurado, D.; Gonthier, E.; Tremel, K.; Kayunkid, N.; Zaborova, E.; Crespo-Monteiro, N.; Boyron, O.; Leclerc, N.; Ludwigs, S.; Brinkmann, M. High-temperature rubbing: a versatile method to align π -conjugated polymers without alignment substrate. *Macromolecules* **2014**, *47*, 3871.
- (60) Li, Q.; Peer, A.; Cho, I. H.; Biswas, R.; Kim, J. Replica molding-based nanopatterning of tribocharge on elastomer with application to electrohydrodynamic nanolithography. *Nature Comm.* **2018**, *9*, 974.
- (61) Zhu, G.; Chen, J.; Liu, Y.; Bai, P.; Zhou, Y. S.; Jing, Q.; Pan, C.; Wang, Z. L. Linear-grating triboelectric generator based on sliding electrification. *Nano Lett.* **2013**, *13*, 2282.
- (62) Grzybowski, B. A.; Winkleman, A.; Wiles, J. A.; Brumer, Y.; Whitesides, G. M. Electrostatic self-assembly of macroscopic crystals using contact electrification. *Nature Mater.* **2003**, *2*, 241.
- (63) Stöhr, J.; Samant, M. G. Liquid crystal alignment by rubbed polymer surfaces: a microscopic bond orientation model. *J. of Electron Microscopy and Related Phenomena* **1999**, *98*, 189.
- (64) Wei, X.; Hong, S.-C.; Zhuang, X.; Goto, T.; Shen, Y. R. Nonlinear optical studies of liquid crystal alignment on a rubbed polyvinyl alcohol surface. *Phys. Rev. E* **2000**, *62*, 5160.

Graphical TOC Entry

